Energy Transfer from Silica Core−Surfactant Shell Nanoparticles to Hosted Molecular Fluorophores†

Enrico Rampazzo,‡ Sara Bonacchi,‡ Riccardo Juris,‡ Marco Montalti,*,‡ Damiano Genovese,‡ Nelsi Zaccheroni,‡ Luca Prodi,*,‡ Diana Cristina Rambaldi,‡,§ Andrea Zattoni,‡,§ and Pierluigi Reschiglian‡,§

Department of Chemistry "G. Ciamician", University of Bologna, via Selmi 2, 40126 Bologna, Italy, and Interuniversity Consortium of Structural and System Biology, INBB, Rome, Italy

Received: March 15, 2010; Revised Manuscript Received: June 18, 2010

Very monodisperse water-soluble silica core−surfactant shell nanoparticles (SCSS NPs) doped with a rhodamine B derivative were prepared using micelles of F127 as nanoreactors for the hydrolysis and condensation of the silica precursor tetraethoxysilane (TEOS). The functionalization of the rhodamines with a triethoxysilane group allowed the covalent binding of the fluorophores to the silica core: no leaking of the dye was observed when the NPs were purified either by ultrafiltration (UF) or dialysis. The diameter of the core ($d_c = 10 \pm 1$ nm) was determined by TEM and subtracted from the hydrodynamic diameter, measured by DLS, ($d_H = 24$ nm, PdI = 0.1) to calculate the shell thickness (∼7 nm). The presence of a single population of NPs with a radius compatible with the one measured by DLS after UF was confirmed by AF4-MALS-RI measurements. The concentration of the NPs was measured by MALS-RI. This allowed us to determine the average number of rhodamine molecules per NP (10). The ability of the NPs to host hydrophobic species as cyanines in the SS was confirmed by fluorescence anisotropy measurements. Steady-state and time-resolved fluorescence measurements allowed us to observe the occurrence of a very efficient Förster resonance energy transfer process from the covalently linked rhodamines to the hosted cyanines. In particular, the analysis of the TCSPC data and steady-state measurements revealed that the adsorption of a single cyanine molecule causes an almost complete quenching of the fluorescence of the NP. Thanks to these observations, it was possible to easily determine the concentration of the NPs by fluorescence titration experiments. Results are in good agreement with the concentration values obtained by MALS-RI. Finally, the hosted cyanine molecule could be extracted with (±)-2-octanol, demonstrating the reversibility of the adsorption process.

Introduction

Silica-based nanostructures represent an extremely versatile and effective platform for the organization of molecular units.[1–11] The properties of the resulting architectures are mostly determined by two factors: (i) the effect of the nanoenvironment on the behavior of each molecular component[2a,b,4e,6b,c] and (ii) the strength of the intercomponent interactions.[1,3c,f,6] Several examples have been reported in the literature that show how fluorescence quantum yield and photostability of fluorescent molecular species can be improved simply by including them in silica nanoparticles (NPs).[2] Segregation of the fluorophores in the silica matrix in fact strongly reduces their interaction with the solvent as well as their excited-state conformational mobility and their accessibility to the atmospheric oxygen.[6b] The combination of these factors in most cases inhibits nonradiative decay processes and prevents photoreactions that could cause the irreversible degradation of the dyes. In addition, the water compatibility of silica NPs allows them to "solubilize" by their inclusion a large variety of molecular hydrophobic species that present a very low solubility in water. Besides the specific effect on the properties of each single fluorophore due to the segregation into the nanostructure, it is worth remembering that silica NPs are individual multichromophoric nano-objects whose overall photophysical behavior depends, as in the case of rigorously supramolecular systems,[1a,12] on the kind and on the strength of the interactions between the molecular units either at the ground or at the excited state.[12–14] In the simplest case, that is, in the absence of any kind of intramolecular interaction, the photophysical features of each NP are simply the combination of those of the trapped molecules. Even this trivial effect has important applicative implication: the presence of a large number of absorbing moieties in a single NP enormously increases the probability that at least one of them is excited upon irradiation. The molar absorption coefficient of heavily doped NPs is hence often extraordinarily higher than the one of molecular species. This feature, combined with its high fluorescence quantum yields, bestows, on a single NP, a much higher brightness[15] than the one typical of molecular dyes. Silica NPs are hence, for their high brightness, low intrinsic toxicity of their composition, and optical transparency, ideal for application in fields of high impact such as medical diagnostics and imaging both in vitro and in vivo.[2d,3a–c,4a–d,g]

A further step toward more sophisticated nanosystems requires the combination of different molecular component according to an already mentioned supramolecular approach. In this context NPs become a rigid skeleton that can be decorated with active molecules to make them "communicate" with each other. In such perspective, the control of the intermolecular interaction between the components is crucial to tune the overall

† Part of the "Michael R. Wasielewski Festschrift".

* Corresponding authors. E-mail: marco.montalti2@unibo.it (M.M.); luca.prodi@unibo.it (L.P.).

‡ University of Bologna.

§ Interuniversity Consortium of Structural and System Biology.

10.1021/jp1023444
Published on Web 07/13/2010

SCHEME 1: Schematic Representation of the Synthesis of NPs $R_{0.25\%}$ (b) using F127 Micelles as Template (a), and Added C Molecules Are Hosted by the NPs (c) and Quench the Rhodamine Fluorescence by FRET

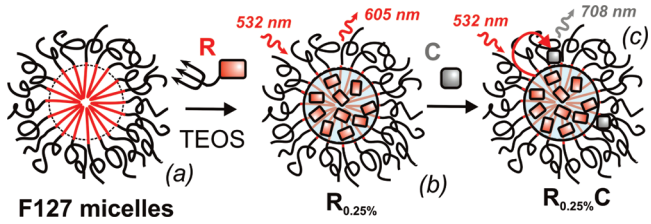

properties of the system. Tan and coworkers reported that this approach is suitable for the design of barcoded fluorescent nanosized labels.[3c] The emission profile of those systems could be controlled by mixing different dyes in silica NPs prepared with the hydrolysis−condensation method developed by Stöber[8] and readapted by Van Blaaderen to introduce fluorescent units in the silica structure.[9] In particular, Tan and coworkers[3c] exploited Förster resonance energy transfer (FRET)[13] between the fluorophores copolymerized in the colloids to tune the different spectral components of the emission to achieve a set of NPs suitable for multiplexed analysis. In two previous papers, we reported that NPs prepared with the Stöber method can be functionalized on the surface with fluorescent silanes.[6a,f] We demonstrated that also in these structures, different from those prepared by Tan including the dyes during the NPs growth, energy and electron transfer processes between the grafted molecules are possible. This same strategy based on surface modification was exploited by Mancin and coworkers to couple a fluorophoric unit to a receptor to achieve fluorescent nanosensors for copper ions.[10b,c]

The scope of this article is to demonstrate that a new kind of silica NPs, different from those traditionally prepared by readapting the Stöber synthesis or alternatively by reverse microemulsion methods,[3a] can be used as a scaffold to organize and to connect molecular components electronically. We prepared these NPs by using the micelles of a surfactant, the Pluronic F127, as a nanoreactor for the hydrolysis−condensation reactions of the silica precursor tetraethoxysilane (TEOS) in an aqueous environment (Scheme 1).[5a,7] The silica growth process is then terminated by the addition of chlorotrimethylsilane (TMSCl), and the NPs can be purified by either ultrafiltration (UF) or dialysis. The dynamic light scattering (DLS) measurements carried out on these NPs show that their hydrodynamic radius is considerably greater than the diameter of the silica core (SC) measured by transmission electron microscopy (TEM) and is comparable to the hydrodynamic radius of the micelles used as template. Such difference indicates that part of surfactant F127 is trapped in the silica during its growth. The presence of this surfactant shell (SS) around the SC makes these SCSS NPs extremely stable in water: no aggregation is observed even several months after their preparation. The use of the micelles as a template allows us to prepare extremely monodisperse samples. The lack of aggregation and the monodisperse character of the NPs was confirmed by asymmetrical flow field-flow fractionation (AF4) online coupled to multi-angle light scatterng detection (MALS). In a previous paper, we have demonstrated that when the synthesis is carried out in the presence of a hydrophobic compound, this last species is trapped in the SCSS NPs and is not released even after UF of the sample.[5a] In this article, we show that: (i) a water-soluble fluorescent molecule such as rhodamines B can be covalently bound to the SC if properly functionalized with a triethoxysilane group (compound **R**, Scheme 2);[11] (ii) preformed and purified SCSS NPs are still able to host in their shell hydrophobic species such as cyanines molecule (compound **C**, Scheme 2); (iii) excitation energy transfer from the covalently linked dye (**R**) to the hosted one (**C**) occurs very efficiently (Scheme 1). Moreover, because no leakage of **R** was observed during the UF, we could determine the molar absorption coefficient of this dye in the NPs and the average number of fluorescent molecules per NP. This latter, very important parameter, has been rarely reported for any kind of doped silica NPs, and it has been calculated via a mostly indirect way. Its experimental determination requires the simultaneous direct measurement of the concentration of the dye and of the NPs in the same solution. General and versatile methods to determine NP concentration in terms of the number of NPs per unit volume are still a major challenge. In this study, a method based on static LS measurements was developed to determine the NP molar mass and consequently the NP concentration in the studied samples. The adsorption of the cyanine **C** in the NPs was demonstrated by fluorescence anisotropy (r) measurements:[14] at low concentration, the value of r for the cyanine is very close to the fundamental value, as expected in the case of a very limited rotational mobility because of the entrapment in a structure (the NP) with a high momentum of inertia. As far as FRET is concerned, the process was investigated by both steady-state and time-resolved fluorescence experiments. In particular, time-correlated single photon counting (TCSPC) experiments demonstrated that the adsorption of a single molecule of **C** causes an almost complete quenching of the fluorescence of the rhodamines in the host NP. Thanks to this observation, the fluorescence titration experiment could be used to determine the concentration of the NP measurements, giving results in perfect agreement with those obtained by LS.

Experimental Section

Chemicals. All reagents and solvents were used as received without further purification: nonionic surfactant Pluronic F127, tetraethoxysilane (TEOS, 99.99%), TMSCl (≥98%), hydrochloric acid (fuming, ≥37%), trimethylaluminum ($AlMe_3$, toluene solution 2.0 M), rhodamine B base (>98%), reagent grade dimethylformamide (DMF), and diethyl ether (Et_2O) were purchased from Aldrich. Piperazine (≥98.0%), triethylamine (≥99.5%), 3-(triethoxysilyl)propyl isocyanate (≥95%), reagent grade dichloromethane, *i*-propyl alcohol, and NaCl were purchased from Fluka. A Milli-Q Millipore system was used for the purification of water (resistivity ≥18 MΩ).

Synthesis of 1 from Rhodamine B Base. The experimental procedure followed for the synthesis of **1** is the one reported by Nguyen and Francis.[16] ^{1}H NMR (250 MHz, [D_3]MeOH, 25 °C, TMS, δ): 1.32 (t, 12H, J = 7.3), 3.14 (br s, 4H), 3.66−3.72 (m, 12H), 6.97−6.98 (d, 2H, J = 2.2), 7.08−7.13 (dd, 2H, J = 2.1), 7.25−7.29 (d, 2H, J = 9.8), 7.50−7.54 (m, 1H), 7.77−7.82 (m, 3H). ^{13}C NMR (62.9 MHz, [D_3]MeOH, 25 °C, TMS, δ): 13.07, 39.45, 44.21, 47.06, 97.50, 114.66, 115.64, 128.96, 131.42, 131.62, 131.87, 132.32, 132.89, 135.53, 156.57, 156.98, 158.96, 169.25. ESI-MS, m/z (M + H) 511.4. Approximate yield 70%.

Synthesis of the Triethoxysilane Derivative R. In a dried flask under N_2 atmosphere, the tertiary amide **1** (500 mg, 0.91 mmol) and triethylamine (2.02 mL, 14.5 mmol) were dissolved in anhydrous DMF (7.5 mL). 3-(Triethoxysilyl)propyl isocyanate (6.77 mL, 27.4 mmol) in 10 mL of CH_2Cl_2 was then added dropwise to this solution at room temperature under stirring. After 12 h, the reaction mixture was dried under reduced pressure. The obtained solid was solubilized by the addition of

SCHEME 2: Synthesis of the Fluorescent Triethoxysilane R and Chemical Formula of Cyanine C

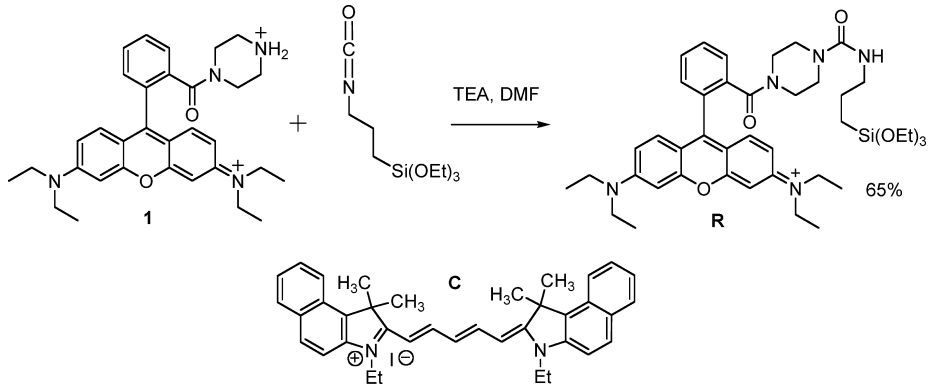

a minimal amount of EtOH and precipitated by dropwise addition of a large volume (~300 mL) of Et_2O. The resulting heterogeneous mixture was cooled under gentle stirring, and the product was obtained by filtration under reduced pressure. The retained dark red-purple solid was rinsed with Et_2O and recrystallized with EtOH/Et_2O.

The product **R** was finally obtained by filtration as a dark red-purple solid, 0.48 gr (yield 65%). ^{1}H NMR (250 MHz, [D_3]MeOH, 25 °C, TMS, δ): 0.59 (t, 2H, J = 8.1 Hz), 1.19 (t, J = 7.3 Hz) and 1.33 (t, J = 8.4 Hz) 21H partially overlapped, 1.57 (m, 2H), 3.09 (t, J = 6.9 Hz) and 3.25 (q, J = 7.3 Hz) partially overlapped 8H, 3.40 (br s, 2H), 3.65−3.73 (q, J = 7.3 Hz) and 3.76−3.86 (q, J = 7.3 Hz,) partially overlapped 14H, 6.97 (d, J = 2.6 Hz), 7.05−7.09 (dd, 2H, J = 2.6 Hz), 7.27−7.30 (d, 2H, J = 9.5 Hz), 7.50−7.54 (m, 1H), 7.67−7.79 (m, 3H). ^{13}C NMR (62.9 MHz, [D_3]MeOH, 25 °C, TMS, δ): 8.52, 9.10, 12.88, 18.70, 24.60, 44.54, 46.92, 47.54, 59.46, 97.34, 114.86, 115.46, 128.98, 131.28, 131.77, 132.32, 133.24, 136.62, 139.09, 157.12, 157.19, 159.27, 159.80, 169.50. ESI-MS, m/z (M + H) 758.6.

Nanoparticles Synthesis. We synthesized core−shell silica-PEG (polyethylene glycol) NPs by adapting previously reported procedures.[5a] In a typical preparation, 200 mg of Pluronic F127 and the desired amount of dye (0.004 mmol) were carefully solubilized with 1 to 2 mL of dichloromethane in a 20 mL glass scintillation vial. The solvent was evaporated from the homogeneous solution by means of a gentle nitrogen flow and subsequently under vacuum at room temperature. NaCl (137 mg) was added to the solid residue, and the mixture was solubilized at 30 °C under magnetic stirring with 3100 μL of HCl 0.85 M. TEOS (360 μL, 1.61 mmol) was then added to the resulting aqueous homogeneous solution, followed by TMSCl (20 μL, 0.16 mmol) after 150 min. The mixture was kept under stirring for 20 h at 30 °C before dialysis/UF treatments. The dialysis purification steps were carried out versus water on a precise amount of NPs solution (800 μL) finally diluted to a total volume of 5 mL with water.

Ultrafiltration and Dialysis Experiments. Nanoparticle UF was carried out in a 75 mL stainless steel glass, solvent-resistant, stirred cell purchased from Millipore (47 mm filters). The UF experimental setup included Amicon regenerated cellulose membranes (10 kDa cutoff) and an auxiliary reservoir (800 mL) equipped with a concentration selector valve.

Dialysis was performed versus water at room temperature under gentle stirring with regenerated cellulose dialysis tubing (Sigma, mol wt cutoff >12 000 Da, av diameter 33 mm).

Dynamic Light Scattering. The determination of the NP hydrodynamic diameter distributions was carried out through DLS measurements employing a Malvern Nano ZS instrument with a 633 nm laser diode. Samples were housed in disposable polystyrene cuvettes of 1 cm optical path length using water as solvent. The width of DLS hydrodynamic diameter distribution is indicated by PdI (polydispersion index). In the case of a monomodal distribution (Gaussian) calculated by means of cumulant analysis, PdI = $(\sigma/Z_{avg})^2$, where σ is the width of the distribution and Z_{avg} is average diameter of the particles population, respectively.

Transmission Electron Microscopy Experiments. A Philips CM 100 TEM operating at 80 kV was used. For TEM investigations, a holey carbon foil supported on conventional copper microgrids was dried up under vacuum after deposition of a drop of NPs solution diluted with water (1:50). We obtained the size distribution by analyzing images with a block of several hundred NPs.

MALS-RI and AF4-MALS-RI Measurements. MALS-RI measurements were performed using a DAWN HELEOS 18-angle light scattering (Wyatt Technology) and an Optilab rEX RI detector (Wyatt Technology). Astra V software (Wyatt Technology) controlled the RI and MALS detectors. For batch measurements, the samples were delivered by a syringe pump (kd Scientific, Holliston, MA) at a flow rate of 0.20 mL/min. Four solutions at different concentrations ranging from 0.05 and 0.2 mg/mL were injected for each sample. Each solution was injected three times. For AF4-MALS-RI experiments, the detectors were connected to an Agilent 1100 liquid chromatography system (Agilent Technologies, Palo Alto, CA) equipped with an Eclipse 3 separation system (Wyatt Technology Europe, Dernbach, Germany). The AF4 channel was 350 μm thick and 240 mm long, with a breath decreasing from 16.0 (inlet end) to 4 mm (outlet end). Regenerated cellulose with 10 kDa molar mass cutoff was used as accumulation membrane. The software package Wyatt Eclipse @ ChemStation version B.03.01 (Wyatt Technology Europe) was used to set and control the flow rate values. All samples were analyzed in PBS, pH 7.2 (100 mM phosphate buffer, 250 mM NaCl). The mobile phase was filtered through 0.1 μm membrane filters (Millipore) and degassed by sonication. The deionized water was produced using a Millipore Direct-Q TM. Samples were focused for 2 min at 1.00 mL/min and then eluted at 1.00 mL/min detector flow rate. The cross-flow was set at 1.5 mL/min and then lowered to 0.0 mL/min in 20 min to generate a hydrodynamic field gradient.

Photophysical Measurements. All NP solutions show very weak light scattering and can be treated from the photophysical point of view as any solution of molecular species. DLS measurements show no aggregation of the NPs, even after several months.

UV−vis absorption spectra were recorded at 25 °C by means of Perkin-Elmer Lambda 45 spectrophotometer. Quartz cuvettes

with optical path length of 1 cm were used. The fluorescence spectra were recorded with an Edinburgh FLS920 equipped photomultiplier Hamamatsu R928P. The same instrument connected to a PCS900 PC card was used for the TCSPC experiments. Luminescence quantum yields (uncertainty, ±15%) were determined using rhodamine 101 solution in ethanol as a reference ($\Phi = 1.0$).[17] Fluorescence intensities were corrected for inner filter effects according to standard methods.[17]

All fluorescence anisotropy measurements were performed on an Edinburgh FLS920 equipped with Glan-Thompson polarizers. Anisotropy measurements were collected using an L-format configuration, and all data were corrected for polarization bias using the G-factor.

Four different spectra were acquired for each sample combining different orientation of the excitation and emission polarizers: I_{VV}, I_{VH}, I_{HH}, I_{HV} (where V stands for vertical and H for horizontal; the first subscript refers to the excitation and the second subscript refers to the emission). The spectra were used to calculate the G-factor and the anisotropy r: $G = I_{HV}/I_{HH}$, $r = (I_{VV} - GI_{VH})/I_{VV} + 2GI_{VH}$. For all of the samples, r was mediated in the 700−750 nm spectral range.[14]

Analysis of the Photophysical Data. The efficiency (η_{DR}) of the energy transfer (ET) process from **R** to **C** in $\mathbf{R}_{0.25\%}\mathbf{C}$ (rate constant k_{RC}) can be calculated from the quenching of the rhodamine fluorescence.[18] The ET efficiency is in fact

$$\eta_{RC} = \frac{k_{RC}}{1/\tau_R^0 + k_{RC}} \tag{1}$$

where τ_R^0 is the excited-state lifetime of the rhodamine in the absence of the ET process, namely, in the absence of **C**. The lifetime of rhodamine in the presence of ET is τ_R

$$\tau_R = \frac{1}{1/\tau_R^0 + k_{RC}} \tag{2}$$

hence

$$k_{RC} = \frac{1}{\tau_R} - \frac{1}{\tau_R^0} \tag{3}$$

$$\eta_{RC} = 1 - \frac{\tau_R}{\tau_R^0} \tag{4}$$

$$k_{RC} = \frac{1}{\tau_R^0}\left(\frac{\eta_{RC}}{1 - \eta_{RC}}\right) \tag{5}$$

Equations 3 and 4 can be expressed in terms of fluorescence quantum yield of **R** as $\Phi_R = k_{rad,R}\tau_R'$ or $\Phi_R^0 = k_{rad,R}\tau_R^0$ in the presence or in the absence of the ET ($k_{rad,R}$ is the radiative rate constant of rhodamine)

$$k_{RC} = \frac{1}{\tau_R^0}\left(\frac{\Phi_R^0}{\Phi_R} - 1\right) \tag{6}$$

$$\eta_{RC} = 1 - \frac{\Phi_R^0}{\Phi_R} \tag{7}$$

The corrected fluorescence intensity of rhodamine at a given wavelength can be expressed as $I_R = \gamma\Phi_R A_R$, where A_R is the absorbance of **R** at a given excitation wavelength and γ is an instrumental parameter. Because A_R does not change because of the addition of **C**

$$k_{RC} = \frac{1}{\tau_R^0}\left(\frac{I_R^0}{I_R} - 1\right) \tag{8}$$

$$\eta_{RC} = 1 - \frac{I_R}{I_R^0} \tag{9}$$

The fluorescence spectrum of $\mathbf{R}_{0.25\%}\mathbf{C}$ contains a contribution due to the rhodamine and another contribution due to the cyanine, the relative weight of which depends on the excitation and emission wavelength. Indicating $\alpha_R = \gamma\Phi_R$ and $\alpha_C = \gamma\Phi_C$, the corrected emission intensity in the absence of ET is expected to be

$$I = I_R + I_C \tag{10}$$

where

$$I_R = \alpha_R A_R \tag{11}$$

$$I_C = \alpha_C A_C \tag{12}$$

In the case of weak interaction at the ground state, the total absorption (independently from the efficiency of the ET process) is

$$A = A_R + A_C \tag{13}$$

In the case of ET, eqs 11 and 12 become

$$I_R = \alpha_R(1 - \eta_{RC})A_R \tag{14}$$

$$I_C = \alpha_C(A_C + \eta_{RC}A_R) \tag{15}$$

In the presence of different population having different ET efficiencies $\eta_{RC,i}$, eqs 14 and 15 are still valid if $\eta_{RC}$is replaced by its average value $\langle\eta_{RC}\rangle = \sum_i f_i\eta_{RC,i}$, where f_i is the molar fraction of the ith population. The presence of different populations is due to the fact that during the titration some NPs that do not host any **C** molecule ($\eta_{RC,i} = 0$) and some NPs that have trapped one or more guest molecules ($\eta_{RC,i} > 0$) are simultaneously present. Upon irradiation of $\mathbf{R}_{0.25\%}\mathbf{C}$ at 532 nm, only **R** is excited because the absorbance of **C** is extremely weak. Moreover, α_C is zero in the window between 550 and 650 nm, where the fluorescence of **R** can be selectively detected, and hence $I = I_R = \alpha_R(1 - \langle\eta_{RC}\rangle)A_R$. In particular, to minimize the inner filter effects, it is convenient[17] to monitor the fluorescence at 605 nm, where the total absorbance remains quite

low ($A < 0.03$) during the titration of the NPs with **C**. In the absence of **C**, $I = I_R^0 = \alpha_R A_R$, and it is hence possible to obtain

$$\langle \eta_{RC} \rangle = 1 - \frac{I_R}{I_R^0} \tag{16}$$

Using this equation, we calculated the average ET efficiencies reported in Figure 8. These values obtained on the basis of the quenching of rhodamine fluorescence were than used to calculate, from eq 15, the cyanine fluorescence intensity expected in the case of sensitization upon excitation of the rhodamines.

The TCSPC decay of $\mathbf{R_{0.25}}$ in the absence of **C** was fitted with a biexponential model

$$I(t) = A + B_1 e^{-t/\tau_1} + B_2 e^{-t/\tau_2} \tag{17}$$

where τ_1 and τ_2 are the excited-state lifetime of two different populations of rhodamines in the NPs and the pre-exponential terms B_1 and B_2 are proportional to the radiative constant and to the concentration of the two families of dyes. The decays recorded in the presence of **C** were fitted with a triexponential model keeping $\tau_1$and τ_2 fixed to their initial value

$$I(t) = A + B_1 e^{-t/\tau_1} + B_2 e^{-t/\tau_2} + B_3 e^{-t/\tau_3} \tag{18}$$

The third lifetime term is due to the presence of NPs quenched by **C**. The decrease in the maximum number of counts in the TCSPS decay during the titration clearly indicates that this lifetime value is overestimated (whereas B_3 is underestimated) because of the limited resolution of the instrumental equipment in the subnanosecond range.

To compare the TCSPC result with the steady-state fluorescence measurements

$$I \propto B_1\tau_1 + B_2\tau_2 + B_3\tau_3 \tag{19}$$

Because in the presence of an ET process it is expected that $B_1 + B_2 + B_3$ is constant, we recalculated $B_3 = B_1^0 + B_2^0 - B_1 - B_2$, where B_1^0 and B_2^0 are the pre-exponential terms obtained in the absence of **C**. We can estimate the ET rate constant and efficiency at the end of the titration by replacing in eq 3 the average initial lifetime $\langle\tau\rangle = 2.95$ ns: $k_{rc} = 2.2 \times 10^9$ s^{-1}; $\eta_{rc} = 0.86$.

Results and Discussion

Synthesis and Characterization of NPs. Nanoparticles $\mathbf{R_{0.25\%}}$ were prepared starting from the fluorescent triethoxysilane **R** and using TEOS as silica precursor. Micelles of the surfactant F127 containing the fluorophores were cross-linked in water by the addition of TEOS; the growth of the SC was terminated by the addition of TMSCl. An amount of 0.25% of **R** in moles with respect to TEOS was used for the synthesis. An undoped sample **U** was prepared repeating the synthesis under the same conditions in the absence of rhodamines. The NPs were purified by UF: no significant traces of unreacted fluorophore could be detected in the filtered waste solution of $\mathbf{R_{0.25\%}}$ by spectrophotometric analysis. To confirm the covalent binding of the fluorescent triethoxysilane to the SC, we prepared a third NP sample replacing in the synthesis **R** with the parent compounds

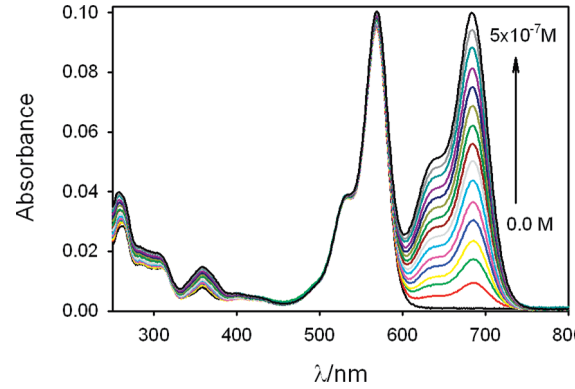

Figure 1. Absorption spectra of a 1×10^{-7} M water solution of NPs $\mathbf{R_{0.25\%}}$ during the titration with **C**. Each variation corresponds to the addition of 3.3×10^{-8} M of **C**.

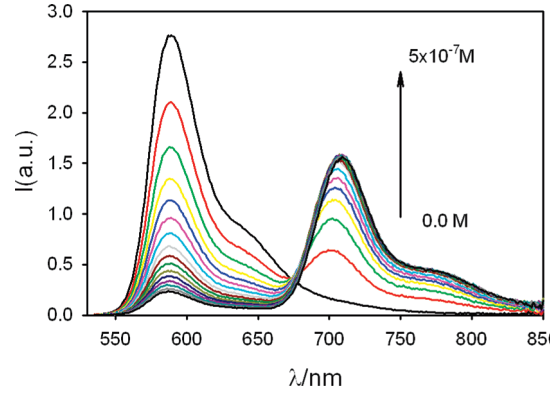

Figure 2. Fluorescence spectra of a 1×10^{-7} M water solution of NPs $\mathbf{R_{0.25\%}}$ during the titration with **C** upon excitation at 532 nm. Each variation corresponds to the addition of 3.3×10^{-8} M of **C**.

1 (Scheme 2), which do not have any function suitable for the covalent binding to the silica and can hence only be physically trapped in the NPs. In this case, more than 90% of **1** was lost during UF whereas only traces of the fluorophore could be observed in the NPs sample. Also, extraction experiments with (±)-2-octanol were performed on the $\mathbf{R_{0.25\%}}$ water solution. No significant traces of the rhodamine could be detected in the organic phase by spectrofluorimetry.

Part of the $\mathbf{R_{0.25\%}}$ NPs solution was diluted with water to determine the molar absorption coefficient of **R** ($\varepsilon_{max} = 1.0 \times 10^5$ M^{-1} cm^{-1} at $\lambda_{max} = 568$ nm) in the NPs. This value coincides with the one measured for **R** in ethanol solution despite the fact the position of the maximum under these conditions is slightly blue-shifted ($\lambda_{max} = 560$ nm). The solution was further diluted to have a sample with absorbance lower than 0.1 in the whole spectral region, as required to record corrected emission and excitation spectra. As shown in Figure 1, the absorption spectrum of the NPs is dominated by the bands of the fluorophores, whereas almost no contribution due to the silica structure can be detected. The solution appeared perfectly clear and could be characterized from the photophysical point of view as any solution of molecular species. As already observed for the absorption, the fluorescence maximum of **R** is also red-shifted (from $\lambda_{max} = 580$ nm in EtOH solution to $\lambda_{max} = 590$ nm in the NPs, Figure 2) because of the entrapment in the silica matrix. The fluorescence quantum yield of the rhodamine in $\mathbf{R_{0.25\%}}$ NPs is $\Phi = 0.35$, whereas its excited-state decay could be fitted with a two exponential model ($\tau_1 = 2.24$ ns, $\tau_2 = 4.63$ ns). The presence of two populations of dyes has been already observed for fluorescein-[6e] and pyrene-doped[6b]

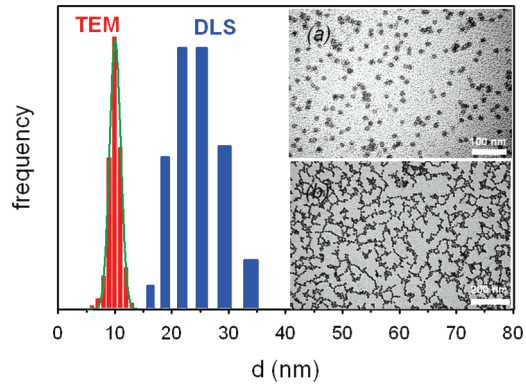

Figure 3. (a,b) Representative TEM images of $\mathbf{R}_{0.25\%}$. The two samples were prepared from a 1×10^{-7} and a 1×10^{-5} M solution of NPs, respectively. The histogram of the diameters obtained from the analysis of the TEM data (red bars) was fitted with a Gaussian distribution (green line). Blue bars are the histogram of the of the diameters obtained from the DLS measurements.

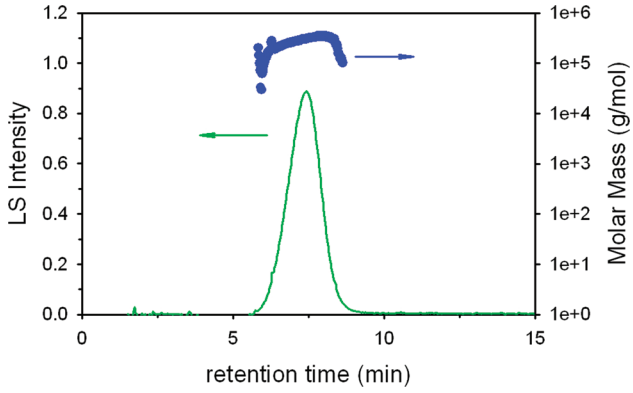

Figure 4. AF4-MALS signal as a function of the detection time for $\mathbf{R}_{0.25\%}$ NPs (green line). The MALS signal was processed in correspondence of the peak to calculate the molar mass of the NPs (blue circles)

NPs prepared with the Stöber method and was explained as being due to some degree of preorganization of the fluorescent triethoxysilane during the NPs growth. Representative TEM pictures of the NPs are shown as Figure 3; only the SCs present enough contrast to be spotted in the images. From the elaboration of the TEM data, we obtained the diagram of the distribution of the diameter of the cores shown in Figure 3. The histogram was fitted according to a Gaussian distribution, allowing us to calculate average diameters of 10 ± 1 nm for the silica nuclea. DLS measurements (Figure 3 inset) were carried out on diluted water solutions of the doped NPs and allowed to calculate a hydrodynamic radius of 12 nm with PdI $= 0.1$. Solutions at different concentrations were injected directly into the RI and MALS detector cells. The dn/dc value was calculated by linear regression of refractive index (n) versus concentration (w/v) values. The obtained dn/dc value was (0.230 ± 0.005) mL/g. The LS signals and the dn/dc value were then used to calculate the NP molar mass by means of the Zimm method.[19] The weight-average molar mass was found to be $(2.539 \pm 0.008)\ 10^5$ g/mol. In Figure 4, the AF4-MALS profile of the NPs is reported. The MALS trace shows a single population of NPs that are eluted at a retention time of ~7.5 min. According to the AF4 theory, the NP average hydrodynamic radius value was determined from the experimental retention time value. Within the typical AF4 reproducibility, the obtained values of 10.5 nm is comparable to the hydrodynamic value obtained by DLS measurements, which is above-

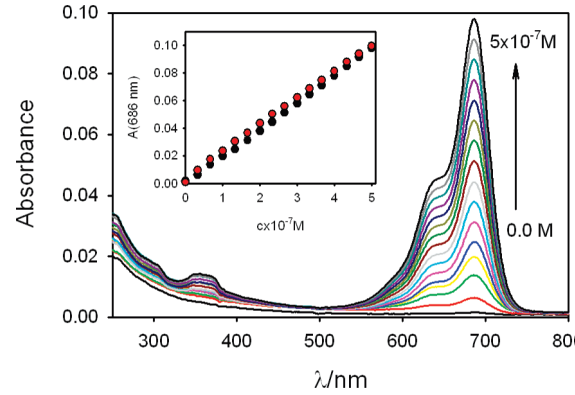

Figure 5. Absorption spectra of a 1×10^{-7} M water solution of undoped NPs **U** during the titration with **C**. Each variation corresponds to the addition of 3.3×10^{-8} M of **C**. In the inset, the absorbances at 686 nm measured during the titration of **U** (black circles) and $\mathbf{R}_{0.25\%}$ (red circles) are compared.

reported. From the MALS signal processed in correspondence of the NP band, the molar mass distribution plot was determined (Figure 4). The polydispersity index (M_z/M_n) was found to be equal to 1.08 (±4%). This is an additional finding that indicates the narrow size distribution of the samples. From the molar mass of the NPs, it was possible to calculate the NP concentration ($c = 1 \times 10^{-7}$ M) of the diluted solution used for the fluorescence measurements and having an absorbance in the maximum of the band of the rhodamines of 0.1 corresponding to a concentration of **R** of 1×10^{-6} M. Comparing the concentration of the dye and of the NPs results that each NP contains an average of 10 fluorophores.

Adsorption of the Cyanine by the Undoped NP U. To check the ability of SCSS NPs of hosting hydrophobic species, we prepared a solution of undoped NP **U** and titrated it by adding very small volumes of an acetonitrile solution of **C**, a dye that presents very low solubility in water. The absorption spectra recorded during the experiments are reported in Figure 5 and show that **C** can be solubilized in water in the presence of the undoped NPs **U**. The different curves in Figure 5 were recorded starting from 3.0 mL of a 1×10^{-7} M water solution of **U** and adding 15 aliquots of 1 μL of a 1×10^{-4} M CH_3CN solution of **C**. The final amount of acetonitrile in the solution was hence very modest (<0.5%, v/v).[20] As shown in Figure 5, the undoped NPs, because of the small size, present a very low extinction coefficient and are completely transparent in the visible region. The shape of the absorption band of **C** does not change, increasing its concentration, and is quite similar to the one observed in CH_3CN solution. The absorption at 686 nm, in particular (Figure 5, inset), increases proportionally to the amount of dye solution added, indicating the absence of a strong interaction between the dye molecules at the ground state in the NP. The molar absorption coefficient of **C** in the NPs is $\varepsilon = 2.0 \times 10^6\ M^{-1}\ cm^{-1}$ at $\lambda_{max} = 686$ nm and is very similar to the one measured in CH_3CN solution. Similarly to the absorbance, the fluorescence intensity upon excitation at 640 nm also increases with the concentration of the dye (Figure 6). Also, in this case, the spectrum profile and fluorescence quantum yield ($\Phi = 0.24$) are quite similar to the ones recorded in acetonitrile. A gradual red shift of the fluorescence maximum and a deviation from the linearity of the dependence of the fluorescence intensity on the concentration can be observed at higher concentration as a result of interactions between excited- and ground-state molecules, which leads to a partial fluorescence quenching (Figure 6, inset). The adsorption of **C** in the undoped NPs is demonstrated by the fluorescence anisotropy measurements,

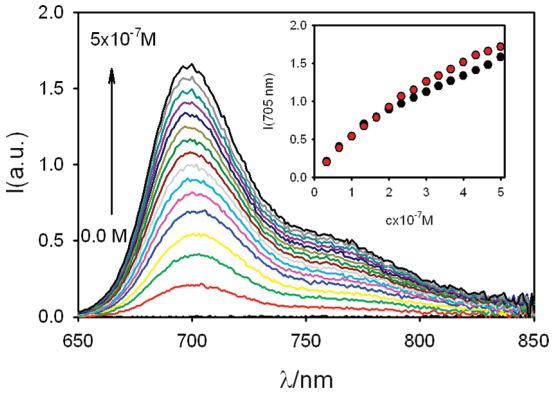

Figure 6. Fluorescence spectra of a 1×10^{-7} M water solution of undoped NPs **U** during the titration with **C** upon excitation at 640 nm. Each variation corresponds to the addition of 3.3×10^{-8} M of **C**. In the inset, the fluorescence intensities at 705 nm measured during the titration of **U** (black circles) and $\mathbf{R}_{0.25\%}$ (red circles) are compared.

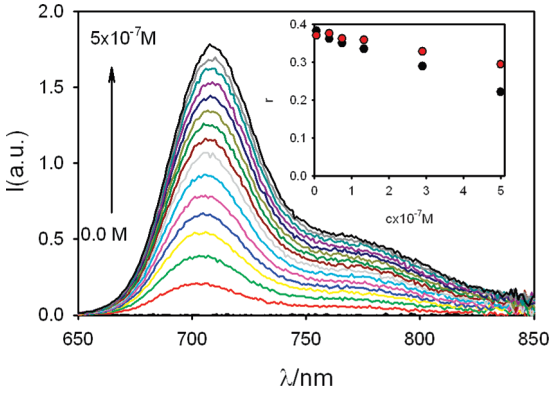

Figure 7. Fluorescence spectra of a 1×10^{-7} M water solution of $\mathbf{R}_{0.25\%}$ NPs during the titration with **C** upon excitation at 640 nm. Each variation corresponds to the addition of 3.3×10^{-8} M of **C**. In the inset, the fluorescence anisotropies measured during the titration of **U** (black circles) and $\mathbf{R}_{0.25\%}$ (red circles) are compared.

which reveal a very low degree of rotational mobility for the dye (at low concentration) in the NPs solution. The inset of Figure 7 shows that when the concentration of the dye is much lower than the one of the NPs the fluorescence anisotropy is very close to its fundamental one (~0.4), indicating that the free rotation of the molecule that would lead to depolarization of the fluorescence is not allowed. This means that the fluorophores are trapped in a high molecular mass structure (the NP), which rotates very slowly in the time range of the decay of the excited state of the molecule. When the concentration of **C** is increased, the population of NPs that hosts more than one fluorophores becomes relevant as well as intermolecular interaction. This is the reason why, as shown in Figure 7, the fluorescence anisotropy is lower at higher dye concentration: in this case, homoenergy transfer processes are responsible for the depolarization.[14]

Adsorption of the Cyanine by the $\mathbf{R}_{0.25\%}$ NPs. The same titration experiment carried out on the undoped NPs **U** with **C** were performed on the doped sample $\mathbf{R}_{0.25\%}$ to investigate the occurrence of a possible ET process from the rhodamine to the cyanine. In this case, excitation was performed either at 532 nm, where the light is predominantly absorbed by the rhodamine dye, or at 640 nm, a wavelength at which only **C** is excited. As already observed for **U**, the addition of **C** to a 1×10^{-7} M solution of NP **R** leads to the appearance, in the absorption spectrum, of the typical band of the cyanine. Figure 1 shows the results of the optical titration: the absorption regions of the

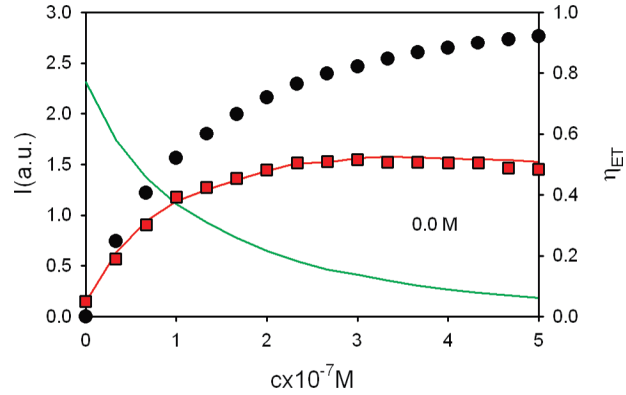

Figure 8. Fluorescence intensity at 605 nm measured during the titration of a 1×10^{-7} M water solution of $\mathbf{R}_{0.25\%}$ NPs with **C** upon excitation at 532 nm (green line) was used to calculate the energy transfer efficiency (black circles). Using such data, the sensitized emission of **C** was calculated (red line) and compared with the experimental data (red squares).

cyanine are similar, for corresponding concentrations, to those observed for the undoped NP **U**. (See also the inset of Figure 5.) No changes of the absorption band of the rhodamine were observed during the titration. The absence of perturbations of the absorption spectra of the two components (**R** and **C**) allows us to rule out the existence of strong ground-state interactions between the dyes. As far as the fluorescence is concerned, the spectra upon excitation of the cyanine ($\lambda_{exc} = 640$ nm, Figure 7) are identical to those recorded during the analog titration of the reference NP **U**. Also in this case, a small red shift and a modest decrease in the fluorescence quantum yield at high concentrations of the dye can be observed because of intermolecular interaction involving excited molecules. Similarly, the dependence of the fluorescence anisotropy on the concentration was the same as that observed in the case of **U**: both the high value of the anisotropy at low concentration and the depolarization due to homoenergy transfer processes at high concentration confirm the adsorption of the **C** molecules in the NPs. On the contrary, as shown by Figure 2 ($\lambda_{exc} = 532$ nm), the presence of the cyanine causes a strong quenching of the fluorescence of the rhodamines. The fluorescence intensity at 605 nm, where only **R** emits light, is plotted in Figure 8 as a function of the concentration of **C**, showing that the quenching efficiency strongly increases with the amount of **C** added to the system. In particular, the fluorescence of **R** is reduced to <10% after the addition of 0.5 equiv of **C** with respect to **R**. It is particularly interesting to note that the first addition of cyanine corresponding to 0.033 equiv of **C** causes a decrease of 30% in the fluorescence of **R**.[21] This observation demonstrates that the adsorption of a single molecule of **C** in an NP causes an almost complete quenching (~90%) of the fluorescence of the rhodamines contained in the SC. Fluorimetric titration can be hence used as an independent method to determine the concentration of SCSS NP solutions. To verify that the quenching was due to an ET process, we compared the fluorescence intensity of the cyanine upon excitation at 532 nm in the presence of the rhodamine with the one recorded for the reference system **U**. Because in both systems the absorbance at the excitation wavelength was quite low (<0.1), no correction of the fluorescence intensity was necessary, and the two signals could be directly compared. The difference between the intensity measured in the two cases is the result of the sensitization of the emission of **C** upon excitation of **R** and definitively demonstrates the occurrence of an ET process from **R** to **C**. To rule out the presence of other different quenching process (such as, for

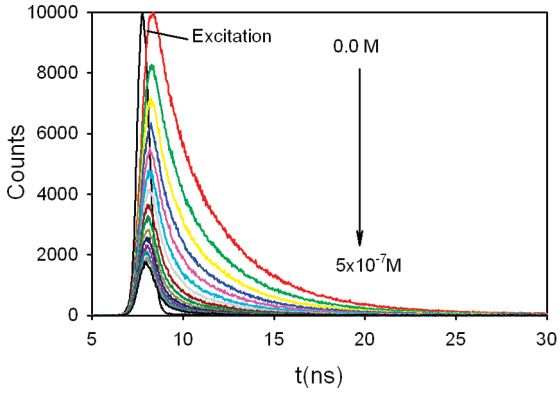

Figure 9. TCSPC profile recorded at 605 nm during the titration of a 1×10^{-7} M water solution of $\mathbf{R}_{0.25\%}$ NPs with **C**. Each variation corresponds to the addition of 3.3×10^{-8} M of **C**.

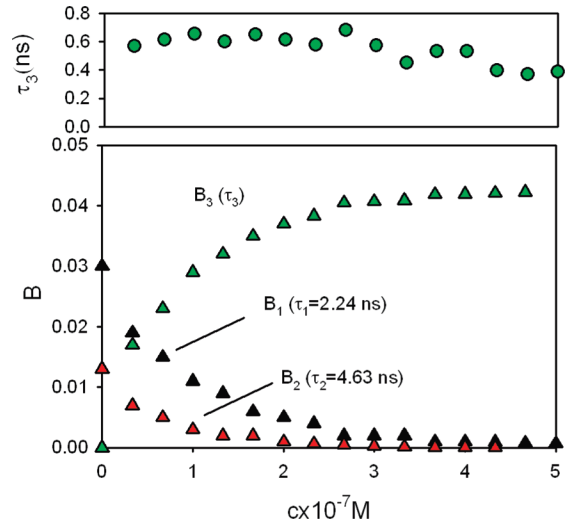

Figure 10. Pre-exponential terms resulting from the triexponential fitting of the TCSPC profile recorded at 605 nm during the titration of a 1×10^{-7} M water solution of $\mathbf{R}_{0.25\%}$ NPs with **C**. τ_1 and τ_2 were maintained fixed to determine the third lifetime τ_3 (green circles).

example, electron transfer), we compared the efficiencies of the quenching of **R** with the efficiency of the sensitized population of the excited state of **C**. The quenching efficiency was calculated using eq 14 and plotted in Figure 8. Such efficiency values were then used to calculate the emission intensity of **C** supposing that quenching was exclusively due to ET using eq 15. As shown in Figure 8, the calculated intensities perfectly fit the experimental data, confirming the occurrence of the ET process and allowing us to rule out the presence of any other kind of quenching mechanism.

To prove the reversibility of the adsorption process, we stirred the solution of $\mathbf{R}_{0.25\%}$ NPs obtained after the titration with an equivalent volume of (±)-2-octanol, a solvent only slightly mixable with water. The cyanine was extracted by the organic phase while the presence of the NPs in water solution was confirmed both by spectrophotometry and DLS.

Fluorescence Time-Resolved Measurements. TCSPC was used as a technique to determine the excited state lifetime. The decay recorded in the absence and in the presence of increasing amounts of **C** is shown in Figure 9 together with the profile of the excitation pulse ($\lambda_{exc} = 405$ nm). As already mentioned, the decay recorded in the absence of cyanine could be satisfactory fitted with a biexponential model (eq 17), giving as a result two excited-state lifetimes $\tau_1 = 2.24$ ns and $\tau_2 = 4.63$ ns. We obtained the curves of Figure 9 during the titration of $\mathbf{R}_{0.25\%}$ with **C** by stopping each accumulation after a fixed time interval (120 s). The strong decrease in the counts in the maximum observed upon the addition of the cyanine is consistent with the occurrence of a very fast deactivation process. The decay profile recorded a few nanoseconds after the excitation pulse is quite independent of the concentration of **C**. This observation was confirmed by the data analysis: using a triexponential model for the decay (eq 18) and maintaining fixed two of the three lifetimes to the value measured for the initial sample, it was possible to satisfactorily fit all of the decay curves. Figure 10 shows that the third resulting lifetime was in all cases in the 0.4 to 0.6 ns interval. Moreover, both of the pre-exponential terms relative to the fixed lifetimes decrease in the presence of **C**, whereas their ratio is quite independent of the degree of quenching. To understand this behavior, it is important to underline that at the beginning of the titration the concentration of **C** is considerably lower than the one on the NPs. Under these conditions, it is very unlikely that a single NP may host more than one cyanine molecule. The concentration of quenched NPs is hence almost identical to the concentration of hosted cyanine molecules. Because the fluorescence anisotropy measurements prove that all of the dye molecules have been adsorbed (at least in the $0-10^{-8}$ M concentration range) it becomes possible to determine the concentration of the NPs occupied by the cyanine moieties using the pre-exponential terms reported in Figure 10. Because the ET process from the rhodamines to the cyanine does not change the radiative constant of the donor, the pre-exponential terms are, in fact, simply proportional to the concentration of the different excited states. After the addition of 3.3×10^{-8} M of **C**, the contribution of the two longer lifetimes decreases about 30%, whereas the weight of the short lifetime becomes about 30% of the total. This observation allows us again in a different way to determine the concentration of the NPs ($c = 1 \times 10^{-7}$ M) independently from the light scattering measurements. By comparing this concentration with the one of the rhodamine in the same solution ($c = 1 \times 10^{-6}$ M) it is finally possible to calculate the average number of such dye in the NPs (10 molecules/NP).

Conclusions

In conclusion, we have demonstrated that SCSS NPs are a very versatile platform for the organization of molecular dyes in water-compatible nanosystems. In particular, functionalization of the fluorophores with a triethoxysilane function allows them to bind covalently (irreversibly) to the SC. Other molecular units, on the other hand, can be adsorbed in the shell of the NPs exploiting simple hydrophobic effects. These second species can be extracted (released) by apolar matrixes. SCSS NPs can hence simultaneously behave as fluorescent labels (for imaging applications) and as carriers for the delivery of hydrophobic compounds (drugs). The efficient "communication" between the active molecules trapped in the core and the hosted species, on the other hand, makes these NPs suitable structures for the design of new materials for light harvesting, signal processing, and energy conversion. Furthermore, we have reported here different and independent methodologies to determine the concentration of NPs and thus the average number of fluorescent molecules per NP, a very important parameter that has been rarely reported for any kind of doped silica NPs.

Acknowledgment. Financial support by MIUR (LATEMAR, FIRB, and PRIN projects), Fondazione Cassa di Risparmio in Bologna, and INSTM (PRISMA).

References and Notes

(1) (a) Descalzo, A. B.; Martínez-Máñez, R.; Sancenon, R.; Hoffmann, K.; Rurack, K. *Angew. Chem., Int. Ed* **2006**, *45*, 5924–5948. (b) Basabe-Desmonts, L.; Reinhoudt, D. N.; Crego-Calama, M. *Chem. Soc. Rev.* **2007**, *36*, 993–1017. (c) Tian, Z.; Shaller, A. D.; Li, A. D. Q. *Chem. Commun.* **2009**, 180–182. (d) Sokolov, I.; Naik, S. *Small* **2008**, *4*, 934–939. (e) Folling, J.; Polyakova, S.; Belov, V.; van Blaaderen, A.; Bossi, M. L.; Hell, S. W. *Small* **2008**, *4*, 134–142. (f) Teolato, P.; Rampazzo, E.; Arduini, M.; Mancin, F.; Tecilla, P.; Tonellato, U. *Chem.—Eur. J.* **2007**, *8*, 2238–2245. (g) Prodi, L. *New J. Chem.* **2005**, *29*, 20–31. (h) Zhong, W. W. *Anal. Bioanal. Chem.* **2009**, *394*, 47–59.

(2) (a) Herz, E.; Ow, H.; Bonner, D.; Burns, A.; Wiesner, U. *J. Mat. Chem.* **2009**, *19*, 6341–6347. (b) Larson, D. R.; Ow, H.; Vishwasrao, H. D.; Heikal, A. A.; Wiesner, U.; Webb, W. W. *Chem. Mater.* **2008**, *20*, 2677–2684. (c) Ow, H.; Larson, D. R.; Srivastava, M.; Baird, B. A.; Webb, W. W.; Wiesner, U. *Nano Lett.* **2005**, *5*, 113–117. (d) Burns, A.; Ow, H.; Wiesner, U. *Chem. Soc. Rev.* **2006**, *35*, 1028–1042.

(3) (a) Wang, L.; Lofton, C.; Popp, M.; Tan, W. *Bioconjugate Chem.* **2007**, *18*, 610–613. (b) Yan, J. L.; Estevez, M. C.; Smith, J. E.; Wang, K. M.; He, X. X.; Wang, L.; Tan, W. H. *Nano Today* **2007**, *2*, 44–50. (c) Smith, J. E.; Wang, L.; Tan, W. T. *Trends Anal. Chem.* **2006**, *25*, 848–855. (d) Wang, L.; Tan, W. H. *Nano Lett.* **2006**, *6*, 84–88. (e) Yao, G.; Wang, L.; Wu, Y. R.; Smith, J.; Xu, J. S.; Zhao, W. J.; Lee, E. J.; Tan, W. H. *Anal. Bioanal. Chem.* **2006**, *385*, 518–524. (f) Wang, L.; Yang, C. Y.; Tan, W. H. *Nano Lett.* **2005**, *5*, 37–43.

(4) (a) Lee, Y. E. K.; Smith, R.; Kopelman, R. *Annu. Rev. Anal. Chem.* **2009**, *2*, 57–76. (b) Nagl, S.; Schaeferling, M.; Wolfbeis, O. S. *Microchim. Acta* **2005**, *151*, 1–21. (c) Kim, S.; Pudavar, H. E.; Prasad, P. N. *Chem. Commun.* **2006**, 2071–2073. (d) Buck, S. M.; Koo, Y. E. L.; Park, E.; Xu, H.; Philbert, M. A.; Brasuel, M. A.; Kopelman, R. *Curr. Opin. Chem. Biol.* **2004**, *8*, 540–546. (e) Rossi, L. M.; Shi, L. F.; Quina, F. H.; Rosenzweig, Z. *Langmuir* **2005**, *21*, 4277–4280. (f) Rossi, L. M.; Shi, L. F.; Rosenzweig, N.; Rosenzweig, Z. *Biosens. Bioelectron.* **2006**, *21*, 1900–1906. (g) Bharali, D. J.; Klejbor, I.; Stachowiak, E. K.; Dutta, P.; Roy, I.; Kaur, N.; Bergey, E. J.; Prasad, P. N.; Stachowiak, M. K. *Proc. Natl. Acad. Sci. U.S.A.* **2005**, *102*, 11539–11544.

(5) (a) Zanarini, S.; Rampazzo, E.; Bonacchi, S.; Juris, R.; Marcaccio, M.; Montalti, M.; Paolucci, F.; Prodi, L. *J. Am. Chem. Soc.* **2009**, *131*, 14208–14209. (b) Zanarini, S.; Rampazzo, E.; Della Ciana, L.; Marcaccio, M.; Marzocchi, E.; Montalti, M.; Paolucci, F.; Prodi, L. *J. Am. Chem. Soc.* **2009**, *131*, 2260–2267.

(6) (a) Bonacchi, S.; Rampazzo, E.; Montalti, M.; Prodi, L.; Zaccheroni, N.; Mancin, F.; Teolato, P. *Langmuir* **2008**, *24*, 8387–8392. (b) Rampazzo, E.; Bonacchi, S.; Montalti, M.; Prodi, L.; Zaccheroni, N. *J. Am. Chem. Soc.* **2007**, *129*, 14251–14256. (c) Montalti, M.; Prodi, L.; Zaccheroni, N.; Battistini, N.; Marcuz, S.; Mancin, F.; Rampazzo, E.; Tonellato, U. *Langmuir* **2006**, *22*, 5877–5881. (d) Montalti, M.; Prodi, L.; Zaccheroni, N. *J. Mater. Chem.* **2005**, *15*, 2810–2814. (e) Montalti, M.; Prodi, L.; Zaccheroni, N.; Zattoni, A.; Reschiglian, P.; Falini, G. *Langmuir* **2004**, *20*, 2989–2991. (f) Montalti, M.; Prodi, L.; Zaccheroni, N.; Falini, G. *J. Am. Chem. Soc.* **2002**, *124*, 13540–13546.

(7) (a) Huo, Q.; Liu, J.; Wang, L. Q.; Jiang, Y.; Lambert, T. N.; Fang, E. *J. Am. Chem. Soc.* **2006**, *128*, 6447–6453. (b) Liu, Z.; Ding, J.; Xue, J. *New J. Chem.* **2009**, *33*, 88–92.

(8) Stoeber, W.; Fink, A.; Bohn, E. *J. Colloid Interface Sci.* **1968**, *26*, 62.

(9) (a) Van Blaaderen, A.; Imhof, A.; Hage, W.; Vrij, A. *Langmuir* **1992**, *8*, 1514. (b) Verhaegh, N. A. M.; Van Blaaderen, A. *Langmuir* **1994**, *10*, 1427.

(10) (a) Arduini, M.; Mancin, F.; Tecilla, P.; Tonellato, U. *Langmuir* **2007**, *23*, 8632–8636. (b) Arduini, M.; Marcuz, S.; Montolli, M.; Rampazzo, E.; Mancin, F.; Gross, S.; Armelao, L.; Tecilla, P.; Tonellato, U. *Langmuir* **2005**, *21*, 9314–9321. (c) Brasola, E.; Mancin, F.; Rampazzo, E.; Tecilla, P.; Tonellato, U. *Chem. Commun.* **2003**, 3026–3027.

(11) Gao, X. Q.; He, J.; Deng, L.; Cao, H. N. *Opt. Mater.* **2009**, *31*, 1715–1719.

(12) Balzani, V.; Credi, A.; Venturi, M. *Molecular Devices and Machines: Concepts and Perspectives for the Nanoworld*, 2nd ed.; Wiley-VCH: Weinheim, Germany, 2008.

(13) For energy transfer, see, for example:(a) Sapsford, K. E.; Berti, L.; Medintz, I. L. *Angew. Chem., Int. Ed.* **2006**, *45*, 4562–4588. (b) Frigoli, M.; Ouadahi, K.; Larpent, C. *Chem.—Eur. J.* **2009**, *15*, 8319–8330. (c) Guo, M.; Varnavski, O.; Narayanan, A.; Mongin, O.; Majoral, J.-P.; Blanchard-Desce, M.; Goodson, T. *J. Phys. Chem. A* **2009**, *113*, 4763–4771.

(14) Lakowicz, J. R. *Principles of Fluorescence Spectroscopy*; Kluwer Academic/Plenum Publishers: New York, 1999.

(15) The product of the molar absorption coefficient and the fluorescence quantum yield is defined as brightness:Braslavsky, S. E. *Pure Appl. Chem.* **2007**, *79*, 293–465.

(16) Nguyen, T.; Francis, M. B. *Org. Lett.* **2003**, *5*, 3245–3248.

(17) Montalti, M.; Credi, C.; Prodi, L.; Gandolfi, M. T. *Handbook of Photochemistry*; CRC Press: Boca Raton, FL, 2006.

(18) *Topics in Fluorescence Spectroscopy: Principles*. Lakowicz, J. R., Ed.; Plenum Press: New York, 1999; Vol. 2.

(19) Haidar Ahmad, I. A.; Striegel, A. M. *Instrum. Sci. Technol.* **2009**, *37*, 574–583.

(20) The fraction of pure acetonitrile added to both a water solution of **U** and one of $\mathbf{R}_{0.25\%}$ showed no effect on the NP properties.

(21) The 30% quenching is relative to the total intensity variation, that is, the difference between the intensity at the beginning and at the end of the titration.

JP1023444